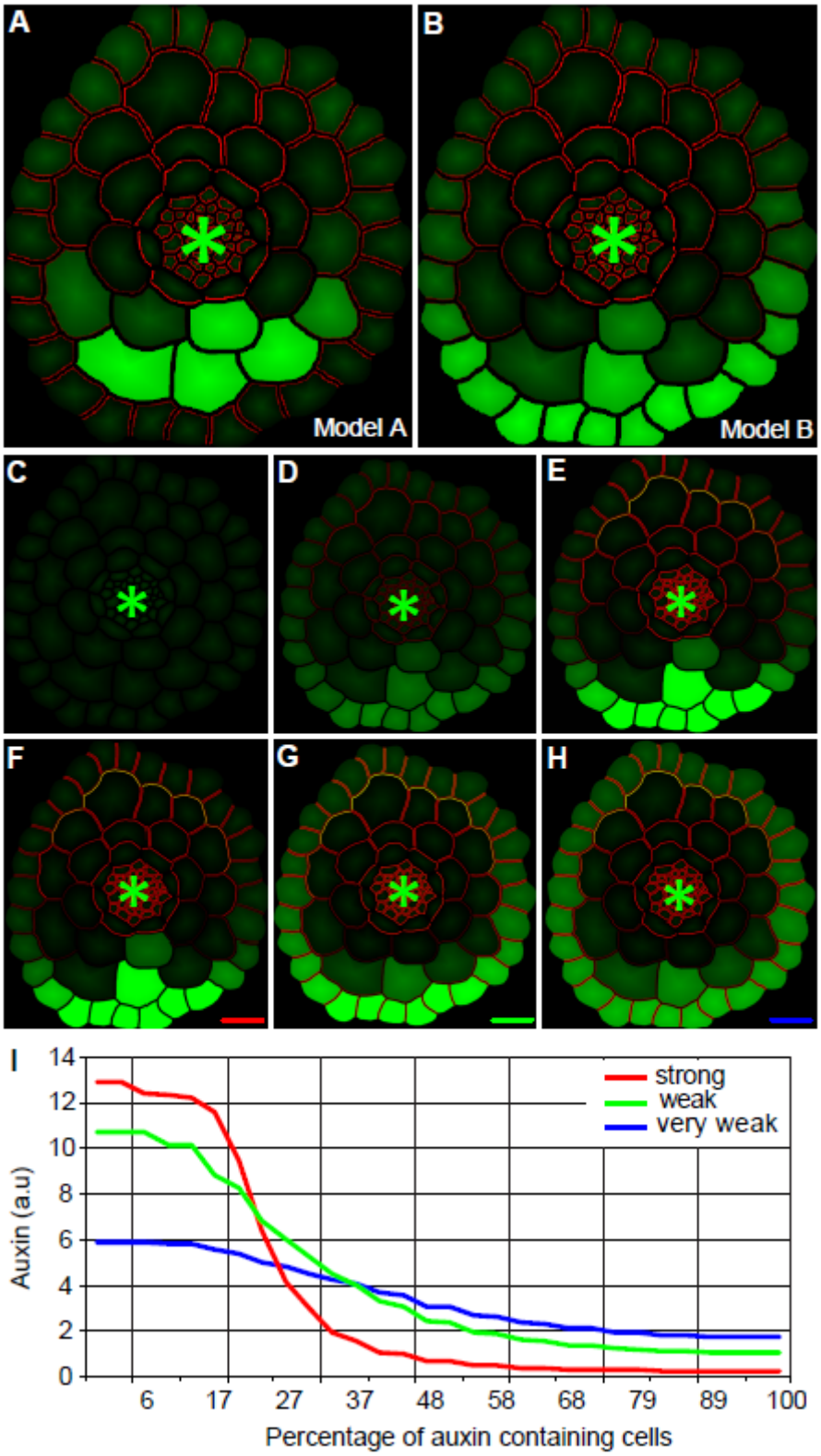

Supplemental Figure 1. Simulated *PIN3* expression and auxin distribution in a cross-section of the apical hook. (A) Increased *PIN3* gene expression solely on the convex side of the cortex tissue leads to preferential auxin accumulation in the cortex at the concave side of the hook (model A). (B) *PIN3* expression in both the cortex and epidermis, leads to preferential auxin accumulation in the epidermis (model B). (C-E) Time-lapse simulations of model B (see also Fig 1A). The initial (C), an intermediate (D) and the steady (E) state are shown. (F-H) Strong (F) to weak (H) differences in combined *PIN4* and *PIN7* expression across the hook epidermis yield sharp to diffused auxin accumulation patterns. (I) Differences in epidermal *PIN4* expression between convex and concave side of the apical hook are relative to the number of auxin-accumulating cells. Color codes for the auxin concentrations and *PIN* expression levels are as in Fig 1C.

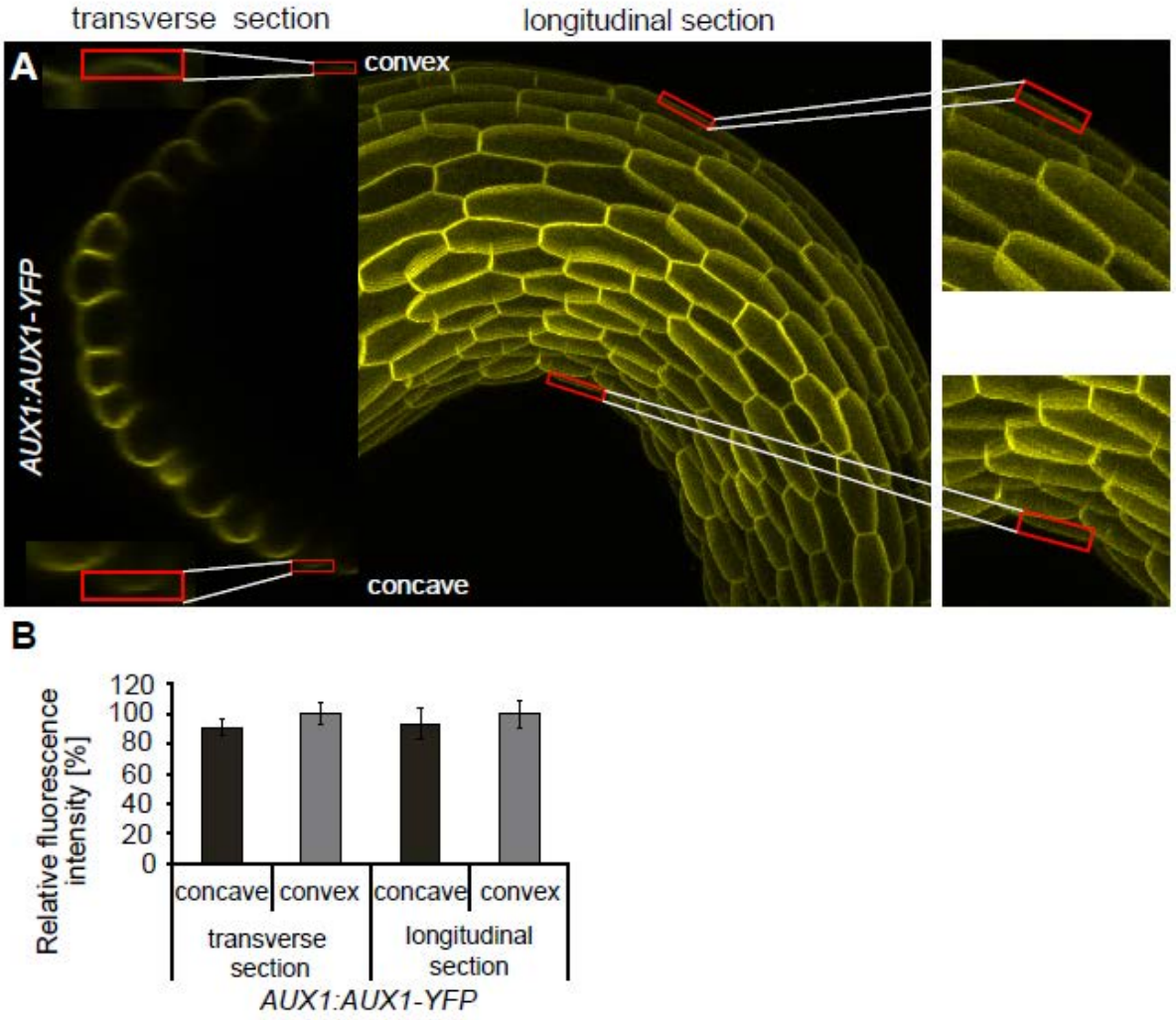

Supplemental Figure 2. **Expression of *AUX1: AUX1-YFP* in the epidermis of apical hooks.**

(A) Expression of the membrane localized AUX1-YFP auxin influx transporter in the epidermis of the apical hook. Membrane AUX1-YFP signal detected in either transverse or longitudinal sections of the apical hook, respectively. Line-scan confocal microscopy and maximal projection of z-stacks images used to acquire images. Insets: close-up of epidermal cells at the convex and concave sides of the apical hook in which membrane AUX1-YFP signal was quantified. (B) AUX1-YFP membrane signal quantified at the concave and convex sides of the apical hook epidermal cells in transverse and longitudinal sections, respectively. Error bars represent standard errors, n = 10 seedlings, at the early maintenance phase 26 hours after germination.

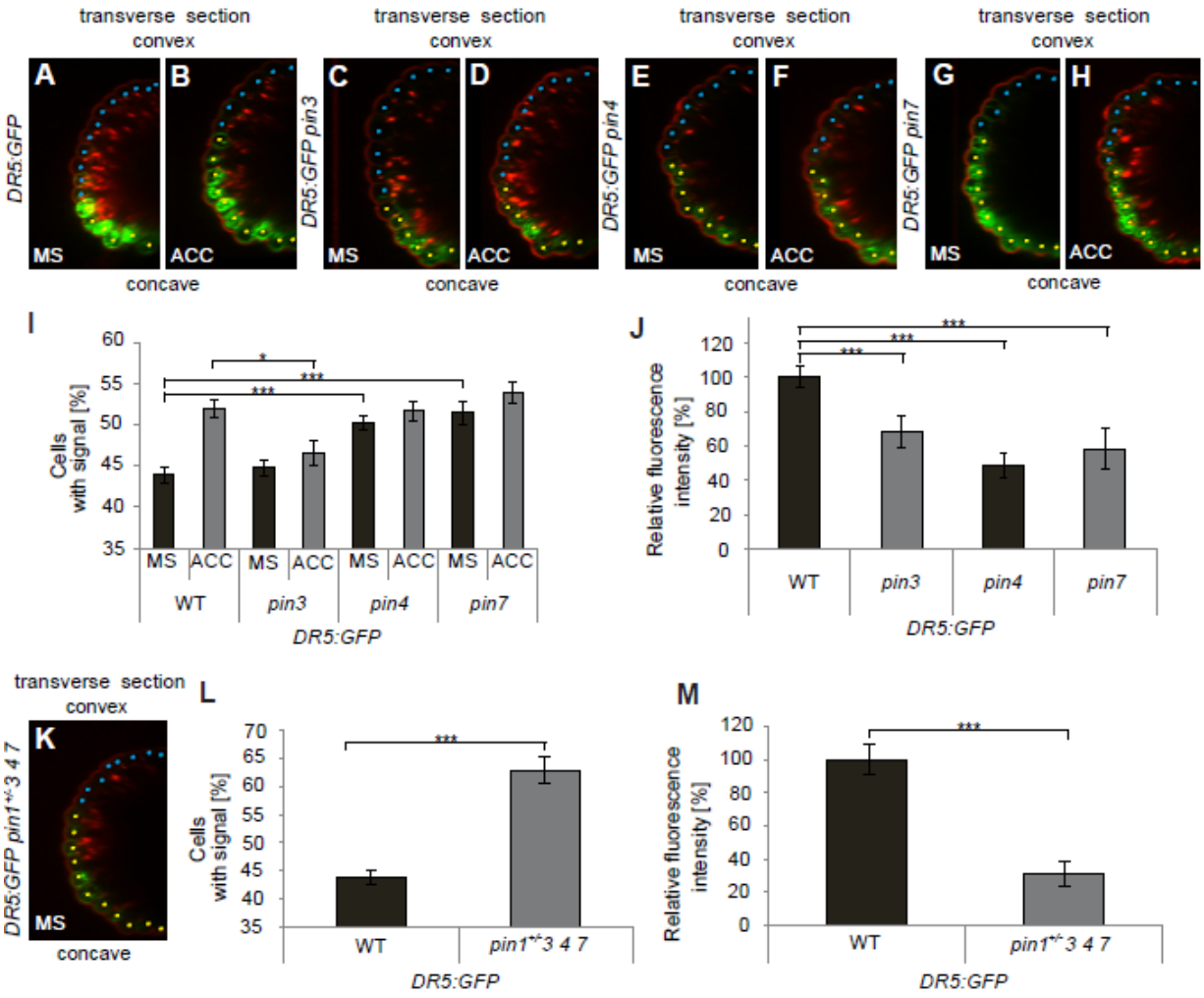

Supplemental Figure 3. PIN-controlled auxin distribution in epidermal cells of the apical hook.

(A-H, K) *DR5rev:GFP* expression monitored in transverse sections of untreated (A,C, E, G,K) and ethylene-treated (B, D, F, H) apical hooks in the wild type (A, B), *pin3* (C, D), *pin4* (E, F), *pin7* (G,H) and *pin1*$^{+/-}$ *pin3 pin4 pin7* (K). (I, L) Scoring of the proportion of the *DR5rev*-positive epidermal cells in untreated and ethylene-treated wild- type, *pin3*, *pin4*, *pin7* (I) and *pin1*$^{+/-}$ *pin3 pin4 pin7* (L) mutant plants. *DR5rev:GFP*-positive cells monitored in transverse sections of the apical hook acquired by line-scan confocal microscopy and maximal projection of z-stacks images. Yellow and blue dots indicate cells with and without *DR5rev*-reporter signal, respectively. Significant differences determined by Student's t-test are indicated as *P < 0.05, ***P < 0.0001, (n = 10 seedlings at the early maintenance phase, 26 hours after germination). (J, M) Quantifications of the *DR5rev*-reporter signal intensity in epidermal cells at the concave side of the hook in wild- type, *pin3*, *pin4*, *pin7* (J) and *pin1*$^{+/-}$ *pin3 pin4 pin7* (M) mutant plants. Significant differences determined by Student's t-test are indicated as ***P < 0.0001 (n = 10 seedlings at the early maintenance phase, 26 hours after germination, GFP signal measured in the epidermal cell at the concave side of the hook). MS, Murashige and Skoog medium; ACC, 5 µM 1- aminocyclopropane-1-carboxylic acid precursor of ethylene. Error bars represent standard errors.

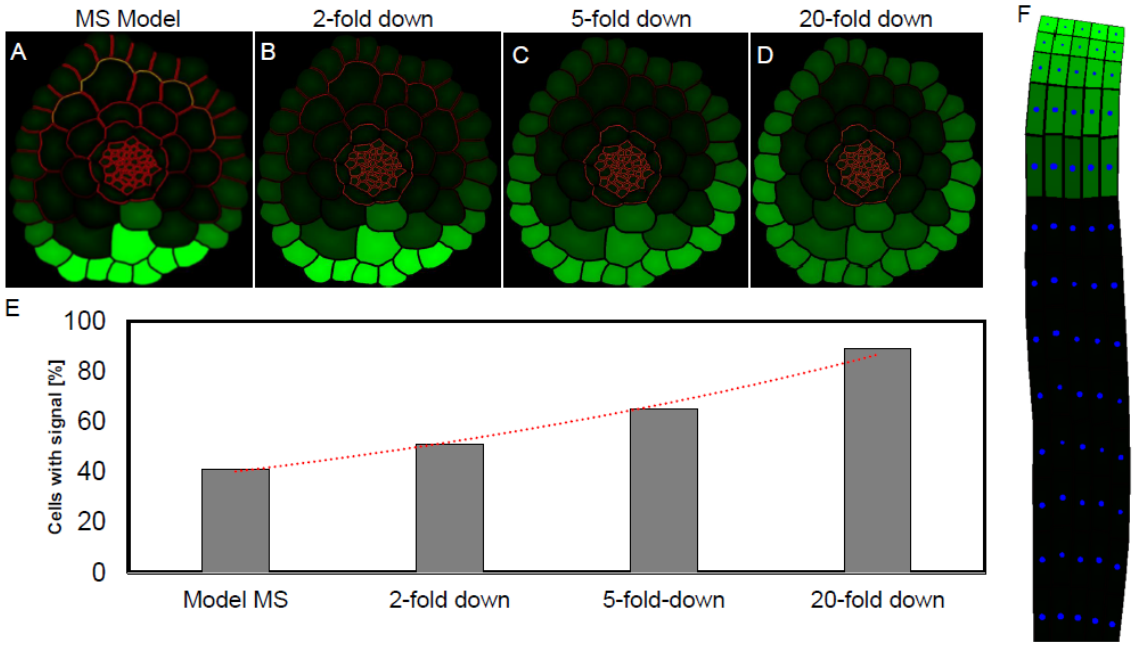

Supplemental Figure 4. Simulation of reduced auxin transport mimics auxin distribution observed in auxin transport mutants.
(A-D) Simulated gradual reduction in auxin transport rates and impact on the auxin distribution in the apical hook. (A) Auxin distribution pattern in the wild-type like seedlings grown on the MS. A two- (B), a five- (C) and a twenty-fold (D) decrease in auxin transport rates results in gradual diffusion of the auxin maxima in epidermis at the concave side of the hook. (E) The weakening of the auxin maxima and increasing percentages of auxin-containing epidermal cells are observed in simulated auxin transport mutants. (F) A hundred-fold reduction in auxin transport rate results in absence of the apical hook and loss of the asymmetric auxin distribution in the hypocotyl. MS - Murashige and Skoog medium.

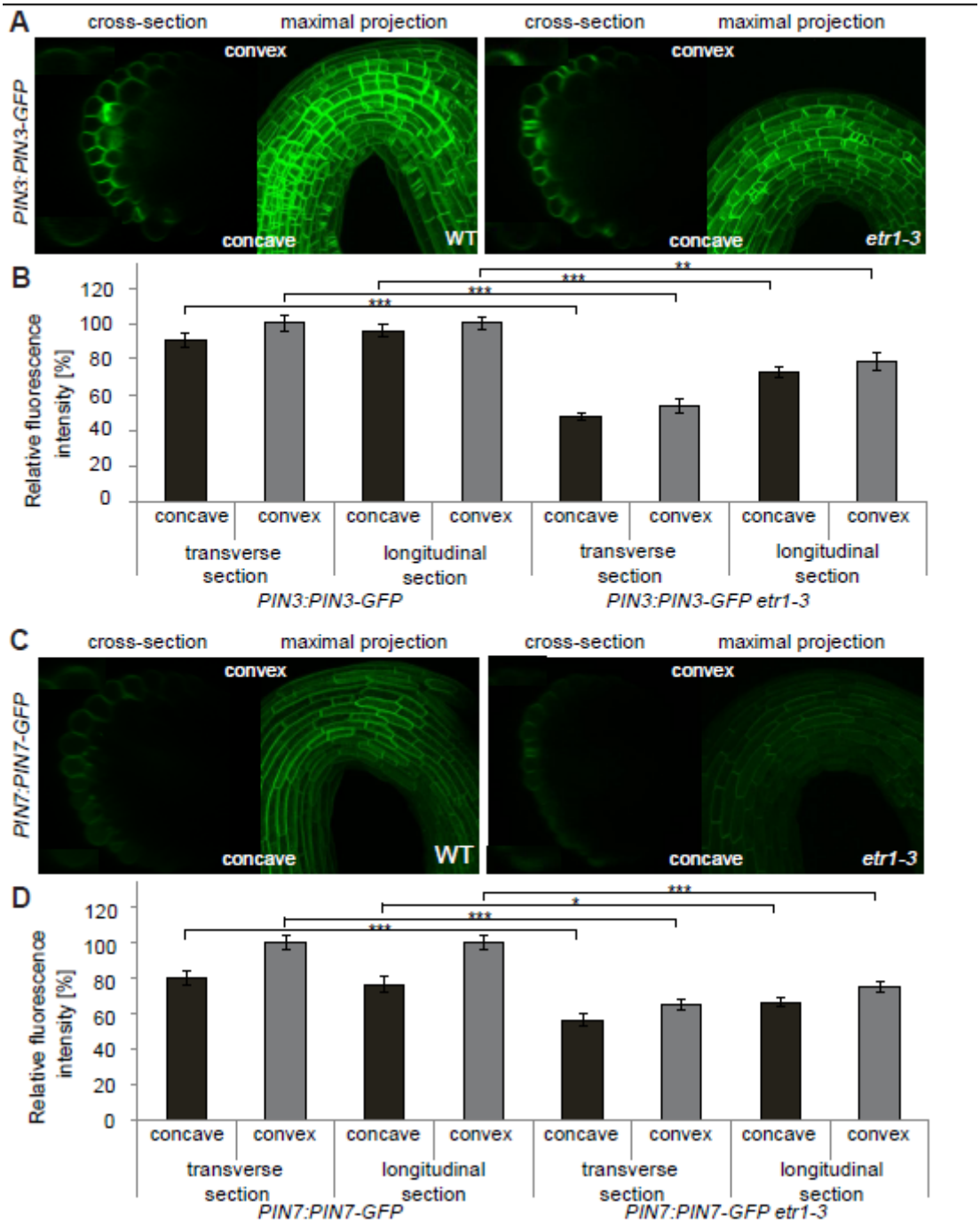

Supplemental Figure 5. Expression of *PIN* auxin efflux transporters in ethylene receptor *etr1-3* mutant. (A - D) Expression of *PIN3: PIN3-GFP* (A) and *PIN7: PIN7-GFP* (C) auxin transporters in the epidermis of apical hooks of the wild type (WT) and *etr1-3* mutant. Membrane PIN-GFP signal in epidermal cells monitored at either the transverse or longitudinal sections of the apical hook, respectively. Line-scan confocal microscopy and maximal projection of z-stack images used to acquire images. PIN-GFP membrane signal was quantified at the concave and convex sides of the apical hook epidermal cells at the transverse and longitudinal sections of the apical hook, respectively (B, D). Significant differences determined by Student's t-test are indicated as *P < 0.05, **P < 0.001, ***P < 0.0001; n = 10 seedlings, at the early maintenance phase 26 hours after germination). Error bars represent standard errors.

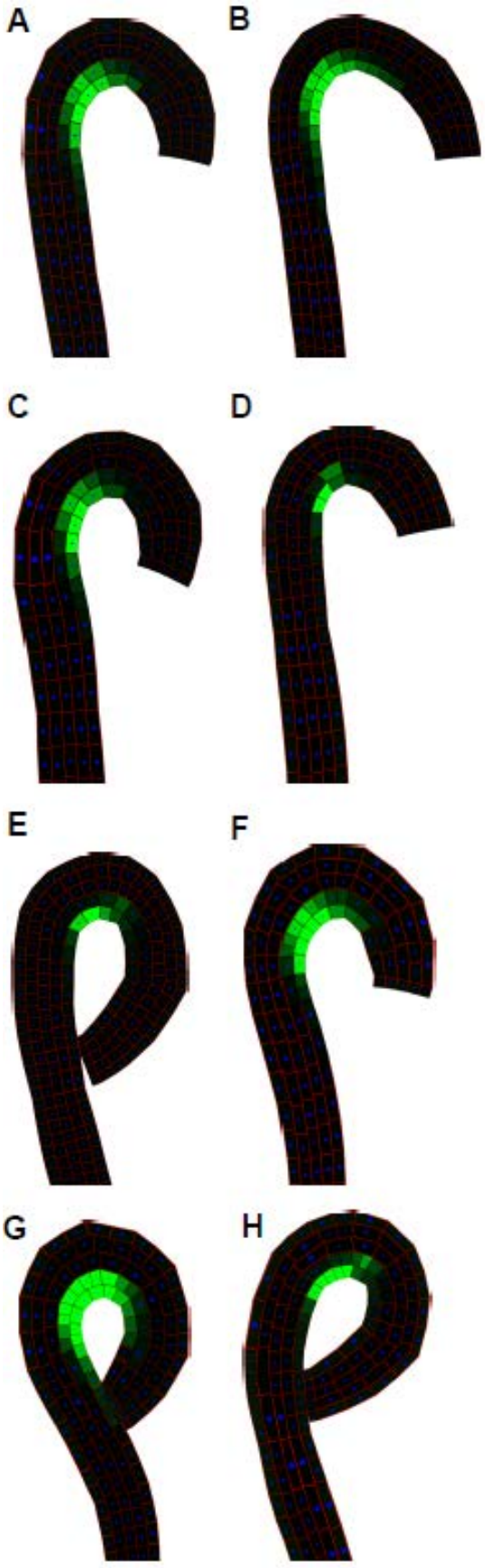

Supplemental Figure 6. Results of simulated formation of the apical hook. The initial stage was represented by the block of cells shown in Fig 3A. (A) Wild type. (B) Weak anisotropy of axial growth. (C) Increased anisotropy of axial growth. (D) Restricted and (E) extended zone of cell proliferation. (F) Simulations of the model integrating auxin-induced cell division and auxin-inhibited cell elongation. (G) Simulation of the effect of ethylene on the increase of auxin levels in the coupled feedback model (F). (H) Same as (G), but with a restricted auxin maximum. Color codes for the auxin concentrations and *PIN* expression levels are as in Fig 1C.

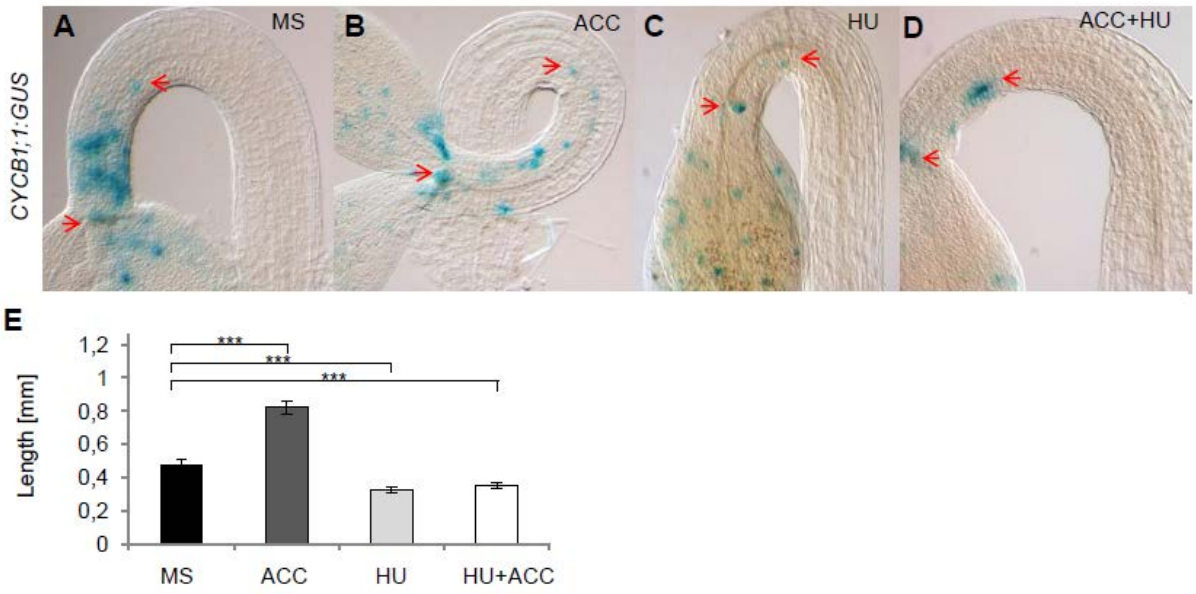

Supplemental Figure 7. Reduced cell proliferation interferes with apical hook formation.

(A-D) *CYC1;1B: GUS* expression during apical hook formation in seedlings grown on MS (A), ACC (B), HU (C), and HU+ACC (D). (E) Quantification of the length of the apical hook zone expressing *CYC1;1B: GUS*. Significant differences determined by Student's t-test are indicated as ***P < 0.0001 (n = 10 seedlings at the early maintenance phase, 26 hours after germination). Red arrows mark zone *of CYC1;1B: GUS* expression. MS, Murashige and Skoog medium; ACC, 5 μM 1-aminocyclopropane-1-carboxylic acid precursor of ethylene; HU, 100 μM hydroxyurea. Error bars represent standard errors.

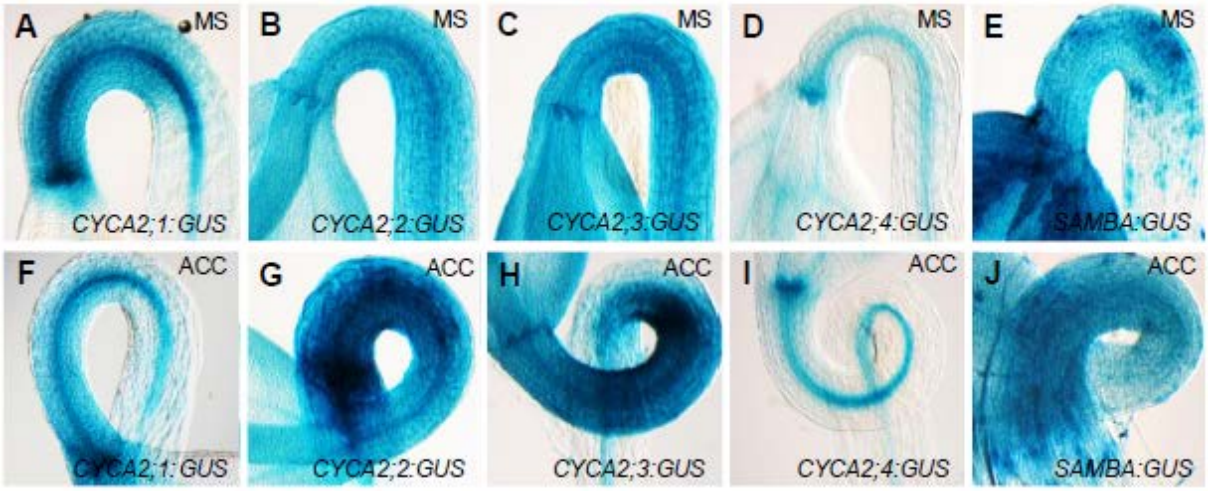

Supplemental Figure 8. Cell cycle-related gene expression in the apical hook. Expression of *CYCA2;1:GUS* (A, F), *CYCA2;2:GUS* (B, G), *CYCA2;3: GUS* (C, H), *CYCA2;4: GUS* (D, I), and *SAMBA: SAMBA-GUS* (E, J) in apical hooks grown on MS and ACC supplemented medium, respectively. MS, Murashige and Skoog medium; ACC, 5 μM 1- aminocyclopropane-1-carboxylic acid precursor of ethylene.

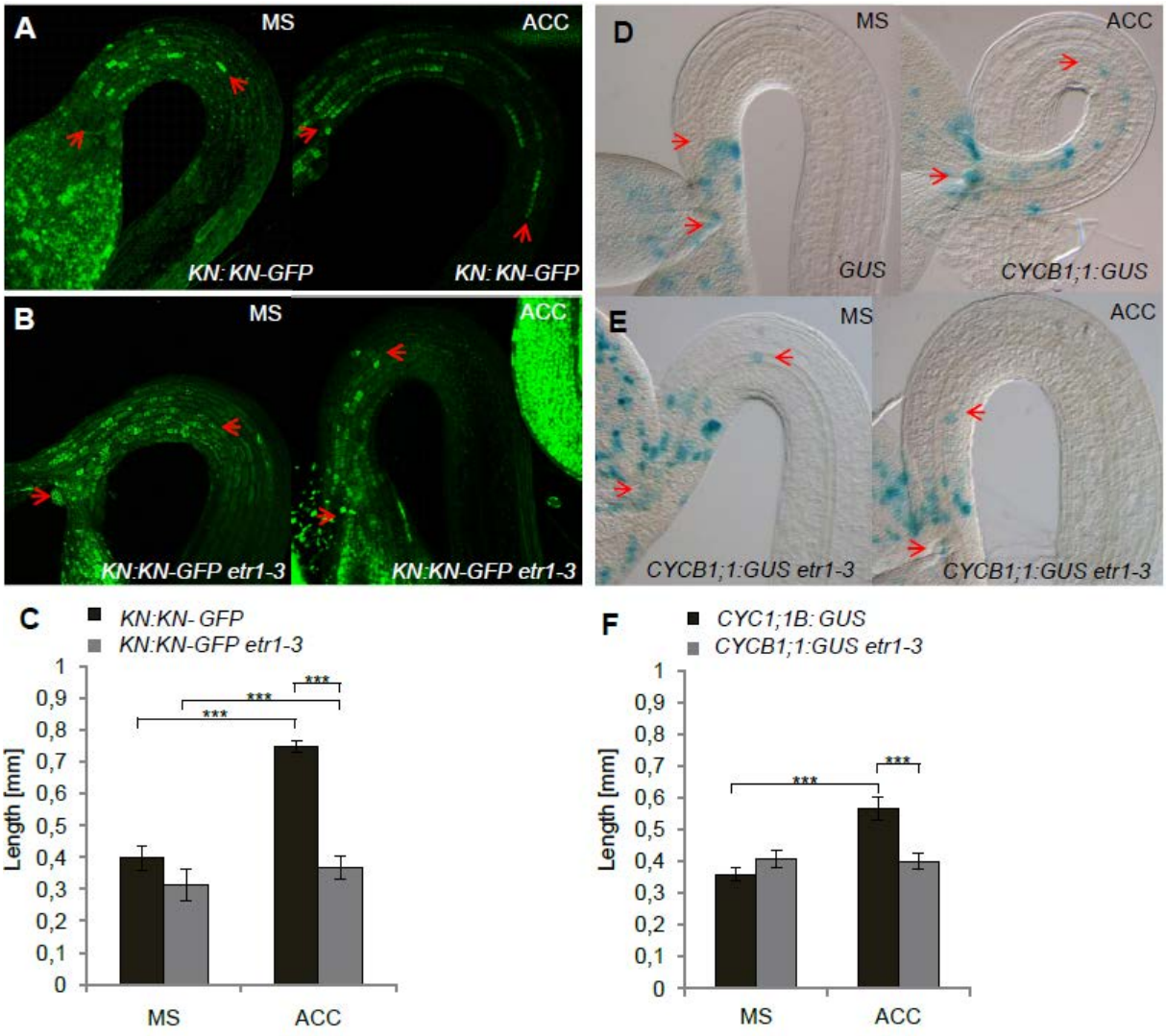

Supplemental Figure 9. Reduced proliferation zone in the ethylene receptor mutant.

(A-E) Cell proliferation activity in control (A, D) and in *etr1-3* (B, E) apical hooks grown on MS and ACC-supplemented medium with the *KN-GFP* (A, B) and *CYC1;1B::GUS* (D, E) reporters. (C, F) Length of the zone expressing *KN-GFP* (C) and *CYC1;1B: GUS* (F) in control and *etr1-3* mutant. Significant differences determined by Student's t-test are indicated as ***P < 0.0001 (n = 10 seedlings at the early maintenance phase, 26 hours after germination). Red arrows mark zone of *KN-GFP* (A, B) and *CYC1;1B: GUS* (D, E) expression. MS, Murashige and Skoog medium; ACC, 5 μM 1-aminocyclopropane-1-carboxylic acid precursor of ethylene. Error bars represent standard errors.

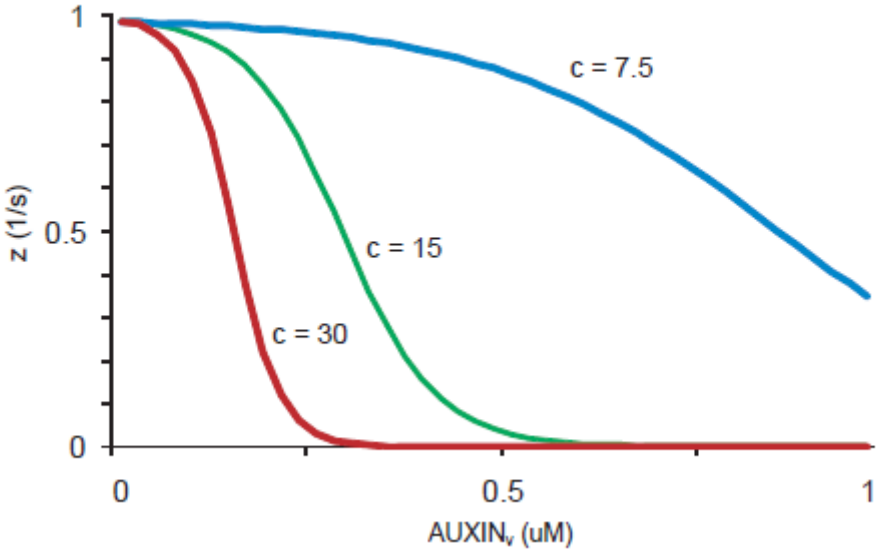

Supplemental Figure 10. Relation between cell growth rate and auxin concentrations.

Sample growth rates calculated using Eq. 16. Parameter values were *a*=1, *b*=0.01 and c=15 (green line) for all simulations presented in Figure 3 and Supplemental Figure 5 with the exception of Supplemental Figure 5B (blue line; c = 7.5) and Supplemental Figure 5C (red line; c=30).

Supplemental Table 1. Expression of *PIN::PIN-GFP* reporters in the epidermis and cortex cells of apical hooks.

Relative expression of *PIN::PIN-GFP* reporters in the epidermis and cortex cells of apical hooks grown on either Murashige and Skoog (MS) or ethylene-supplemented media (ACC). Relative fluorescence intensity of the membrane localized auxin transporters in epidermal and cortex cells detected on longitudinal sections of the apical hook acquired by the maximum projection confocal-based pictures. PIN-GFP signal quantified on transversal membranes of cortex and epidermal cells at concave and convex side of the apical hook, respectively.

PIN3::PIN3-GFP			*PIN4::PIN4-GFP*			*PIN7::PIN7-GFP*		
cortex [%]			cortex [%]			cortex [%]		
	MS	**ACC**		**MS**	**ACC**		**MS**	**ACC**
concave	247,61 (±1,79)	212,87 (±1,62)	**concave**	105,41 (±0,95)	82,53 (±0,73)	**concave**	70,2 (±0,74)	94,08 (±0,65)
convex	325,54 (±2,77)	286,12 (±1,85)	**convex**	163,46 (±1,10)	127,38 (±1,31)	**convex**	85,74 (±0,57)	105,44 (±0,67)
epidermis [%]			epidermis [%]			epidermis [%]		
	MS	**ACC**		**MS**	**ACC**		**MS**	**ACC**
concave	95,85 (±0,84)	83,59 (±0,87)	**concave**	62,63 (±0,83)	33,34 (±0,29)	**concave**	76,52 (±1,00)	115,82 (±1,51)
convex	100 (±0,72)	93,75 (±1,01)	**convex**	100 (±0,95)	58,99 (±0,24)	**convex**	100 (±0,88)	132,39 (±2,00)

100% PIN-GFP-convex in epidermis

Supplemental Table 2. Key model parameter summary.

Model parameter	Value [units]	reference
T_{IAAH} (auxin influx/passive diffusion)	10 [µms^{-1}]; all simulations	[S2, S6, S8]
Φ (auxin production rate)	0.05 [μMs^{-1}]; Supplemental Figure 6G and 6H (mimicking ethylene effect) 0.001 [μMs^{-1}]; all other simulations	assumed in this study
T_{PIN} (auxin efflux)	5 [µms^{-1}]; Figure 2D, 2G, 3J and Figure 3D; 0.2[µms^{-1}] Supplemental Figure 4F 20 [µms^{-1}]; all other simulations	[S2, S6, S8, S9]
μ (auxin turnover)	0.005 [s^{-1}]; all simulations	assumed in this study
a_{PIN} (PIN production rate)	1 [s^{-1}]; all simulations	assumed in this study
β_{PIN} (PIN decay rate)	0.03 [s^{-1}]; all simulations	assumed in this study
η (dimensionless strength of differential PIN expression)	0.5; Supplemental Figure 1G 0.1; Supplemental Figure 1H 1; all other simulations	assumed in this study
K_M (saturation constant)	100 [μM]; all simulations	assumed in this study
k_x (spring stiffness constant)	0.7 [N/μm]; all simulations	assumed in this study
k_b (bending stiffness constant)	1 [N/μm]; all simulations	assumed in this study
δ (dampening coefficient)	0.2 [Ns/μm]; all simulations	assumed in this study
r_b (isotropic growth rate)	0.001 s^{-1};]; all simulations	assumed in this study
D_{hyp} (relative distance from cotyledons; hypocotyl region)	0.2; Supplemental Figure 6D and S6H 0.35; all other simulations	assumed in this study
D_{cot} (relative distance from cotyledons; beginning of hook region)	0.05; all simulations	assumed in this study
D_{div} (relative distance from cotyledons; end of rapid cell proliferation zone)	0.4; Figures 3E and S6E, S6H 0.2; all other simulations	assumed in this study

Supplemental Methods

Digitization of an apical hook cross-section

A high quality, representative cross-section image of an Arabidopsis hypocotyl (PIN3-GFP reporter was used) was loaded into MorphoGraphX (http://www.MorphoGraphX.org) for the extraction of cell membrane positions. After an initial preprocessing (increase in contrast, blurring to remove the noise), the image was manually seeded (i.e., a sample point in each cell was chosen interactively), and this information was used to segment it into cells using a watershed algorithm. After segmentation, a polygonal representation of the cells was used to simulate auxin distributions in the apical hook cross-section using the Vertex-Vertex (VV) simulator in the L-studio environment (http://algorithmicbotany.org/virtual_laboratory/) [S1-S4].

Numerical and simulation methods

We have developed two models of the apical hook. In the first model (Figure 1A) we considered static realistic cellular template obtained from confocal image stacks that represent the transversal cross-section of the hook (digitized hook cross-sections). This transversal hook model was used to simulate the emergence of auxin distribution patterns resulting from differential PIN expression and known fixed PIN localizations. The second model represents a growing array of cells that mimic the longitudinal hook section (longitudinal hook model) (Figure 3). The purpose of this dynamic model was to study how the auxin distribution resulting from the activity of PIN proteins can be translated into differential cell elongation and graded cell proliferation, driving apical hook bending. The array of cells was created using a version of the VV simulator [S1], [S2] embedded in the modeling software L-studio [S3], [S4] (http://algorithmicbotany.org/lstudio). The chemical system was simulated by numerically integrating coupled ODEs, using an adaptive fifth-order Runge-Kutta method [S5]. Cell mechanics (mass-spring system) was simulated using the forward Euler method [S5]. Screenshots from model simulations are shown in Figures 1, 2, and 3, and Supplemental Figures 1 and 5. Final figures were prepared in Adobe Illustrator (Adobe Inc. CS).

Mathematical model description

In the computer model, each cell consists of two compartments, namely the cytoplasm and the plasma membrane. For the sake of simplicity, the extracellular space shared by adjacent cells was not modeled. The plasma membrane is divided into several fragments, each of which faces one of the adjacent cells. Non-polar (diffusive) cell-to-cell auxin transport is modeled as follows:

$$\frac{dAUXIN_i}{dt} = \sigma + \frac{1}{V_i} \cdot \left\{ D_{IAAH} \cdot \sum_{j \in N_i} l_{i->j} \cdot (AUXIN_j - AUXIN_i) \right\} - \mu \cdot AUXIN_i$$

(1)

where $AUXIN_i$ and $AUXIN_j$ are mean auxin concentrations in the cytoplasm of cells *i* and *j*, respectively. V_i and $l_{i->j}$ are the volume of cell *i* and the membrane crossing area between cell *i* and the cell adjacent *j*, respectively. N_i denotes the set of neighbors of cell *i.* The parameter D_{IAAH} represents the plasma membrane permeability for non-polar auxin transport [S6]. The parameter σ is the auxin production, i.e., the auxin source term. It is assumed to be non-zero in the vascular tissue, which is marked by the green asterisk in Figure 1A. In addition, it is non-zero in the most apical cell layer (cotyledons), which is marked by the green bar in Figure 3A. Parameter μ, assumed to be non-zero at the base of the hypocotyl, summarily captures the depletion of auxin due to its transport to the bottom part of the plant (marked by the blue bar in Figure 3A).

The PIN-dependent polar auxin transport is modeled as follows:

$$\frac{dAUXIN_i}{dt} = \frac{1}{V_i} \cdot \left\{ T_{PIN} \cdot \sum_{j \in N_i} l_{i->j} \cdot \left(PIN_j \cdot \frac{AUXIN_j}{1 + AUXIN_j} - PIN_i \cdot \frac{AUXIN_i}{1 + AUXIN_i} \right) \right\} \quad (2)$$

where PIN_i and PIN_j correspond to PIN levels in the adjacent cells *i* and *j*, and T_{PIN} controls PIN-dependent auxin transport across the plasma membrane. We assumed similar transport rates for PIN1, PIN3, PIN4 and PIN7 by setting T_{PIN} to the same non-zero value at the cell membranes at which a PIN signal was observed experimentally. To simulate pin mutants but account for the redundancy between PIN transporters parameter, T_{PIN} was set to ¼ of its default value (Figures 2D, 2G, 2J and 3D). Alternatively, when we assumed a hundred-fold reduction in all PIN transport rates no hook bending could occur (Supplemental Figure 4F). See Supplemental Table 2 for the values used in the model.

Description of PIN expression dynamics

To reflect the experimentally-observed gradual decrease of PIN expression between the convex and concave side of the hook [S10], the asymmetric expressions of PIN3 in the cortex (model A; Supplemental Figure 1A) and PIN4 and PIN7 in the cortex and epidermis (model B; Figures 1A and Supplemental Figure 1B) were described using a function of the position of cell with respect to the concave side of the hook (reference vector (V_g); [x=0, y=1, z=0]. In cross-sectional models we considered two functions:

(a) an angle (in radians) between the vector pointing towards the center of the mass of a given cell (V_c), and the reference vector (V_g) (see Figure 1A):

$$\Delta = (1 - \frac{1}{\pi} \cdot cos^{-1}(\hat{V}_c \cdot \hat{V}_g))$$

(3)

(b) a dot product of V_c and V_g:

$$\Delta = 0.5 \cdot (\hat{V}_c \cdot \hat{V}_g + 1)$$

(4)

Equation 4 provides a better fit to the experimental observations of PIN expression pattern in apical hook cross-sections reported in [S10] than Equation 3. Given the value of Δ, changes in the concentration of PIN were described by the equation:

$$\frac{dPIN_i}{dt} = \frac{a_{PIN} \cdot \eta \cdot \Delta}{1 + K_M \cdot PIN_i} - \beta_{PIN} \cdot PIN_i$$

(5)

where PIN_i is PIN level in i-th cell. Parameters a_{PIN} and β_{PIN} describe basal rates of PIN production and degradation, respectively. The parameter K_M is the saturation rate of PIN expression and the dimensionless parameter η defines the strength of differential PIN protein expression. Equation 5 was used for all PINs used in the simulations. In contrast to PIN3, PIN4 and PIN7, the expression of PIN1 did not depend on Δ. Furthermore, the expression of PIN1 was restricted to the vascular tissues and the endodermis.

In the longitudinal hook model the detailed information regarding the angle between cell position V_c and the reference V_g was not available. Consequently, we used a simplified version of Equation 4, according to which the expression of PIN3, PIN4 and PIN7 was high (Δ=1) on the convex side of the hook, and low (Δ=0) on the concave side (Figure 3A).

Physically-based model of apical hook formation

Cell growth in the apical hook model (Figure 3 and Supplemental Figure 6) is approximated using a mass-spring system [S11-S14]. Each vertex *u* is connected to each of its neighbor vertices *v* by a linear Hookean spring representing a cell wall segment, with a rest length $L_{u,v}$ assumed to be the same for all segments. The magnitude of force exerted by this spring is $k_x \cdot (L_{u,v} - |p_u - p_v|)$ and is positive for spring compression. The k_x characterizes the stiffness of the spring. This force is directed along the direction of the spring $\frac{p_u - p_v}{|p_u - p_v|}$. p_u is the position of vertex *u,* and p_v is the position of neighbor vertex *v.* Therefore, the total force exerted on vertex *u* located at position p_u by all such springs can be written as:

$$F^{u}_{linear} = \sum_{u \in N_u} k_x \cdot (L_{u,v} - |\, p_u - p_v \,|) \cdot \frac{p_u - p_v}{|\, p_u - p_v \,|}$$

(6)

where N_u is the set of vertices adjacent to vertex *u*. The norm symbol indicates the Euclidean distance between the points.

Next, we introduced bending springs to retain the correct shape of cells positioned at the boundary of the modeled tissue against the turgor pressure of the cells pushing towards the hook boundary. These springs respond to changes in the angle $\theta_{u,v,w}$ between three adjacent vertices *u, v, w*. Such an angle is given as in [S13]:

$$\theta_{u,v,w} = cos^{-1}\left(\frac{(p_u - p_v)\cdot(p_u - p_w)}{|p_u - p_v| \cdot |p_u - p_w|} \right)$$

(7)

A bending spring exerts a moment proportional to the difference between the actual angle $\theta_{u,v,w}$ and the rest angle θ_0, i.e, $k_b \cdot (\theta_0 - \theta_{u,v,w}) \cdot \frac{1}{|p_u - p_v|}$ where k_b characterizes the stiffness of the bending spring (assumed to be the same for all springs). This rest angle is assumed to be 90º, consistent with the approximately square shape of the cells in the longitudinal section of the hook. The restoring force must exert a moment, so force acts perpendicular to *v* in the plane of *v* and *w*. The direction of the force is calculated as $\frac{(p_u - p_v)\times[(p_u - p_v)\times(p_u - p_w)]}{|(p_u - p_v)\times[(p_u - p_v)\times(p_u - p_w)]|}$. By combining above formulas and Equation 7 we calculated forces acting on vertices *v* and *w*, respectively, as:

$$F^{v}_{bending} = k_b \cdot (\theta_0 - \theta_{u,v,w}) \cdot \frac{1}{|p_u - p_v|} \cdot \frac{(p_u - p_v)\times[(p_u - p_v)\times(p_u - p_w)]}{|(p_u - p_v)\times[(p_u - p_v)\times(p_u - p_w)]|}$$

(8)

$$F^{w}_{bending} = k_b \cdot (\theta_0 - \theta_{u,v,w}) \cdot \frac{1}{|p_u - p_w|} \cdot \frac{[(p_u - p_v)\times(p_u - p_w)]\times(p_u - p_v)}{|[(p_u - p_v)\times(p_u - p_w)]\times(p_u - p_v)|}$$

(9)

The force acting on central vertex becomes (see also reference [S13]):

$$F^{u}_{bending} = -(F^{v}_{bending} + F^{w}_{bending})$$

(10)

In addition to the forces acting on a vertex due to springs, a force due to the turgor pressure (p_{const}= 0.005) acts in the direction normal to each wall (***n***):

$$F^{u}_{pressure} = p_{const} \cdot \hat{n} \cdot \left| p_u - p_v \right|$$

(11)

Combining the individual force components, the total force acting on a vertex u is

$$F^{u}_{total} = F^{u}_{linear} + F^{u}_{bending} + F^{u}_{pressure}$$

(12)

We used the second Newton's Law of dynamics to calculate the velocity (Vel_u) and position (p_u) of vertex *u* over time for point mass m_u=1:

$$\frac{dVel_u}{dt} = \frac{F^{u}_{total}}{m_u} - \beta \cdot Vel_u$$

(13)

$$\frac{dp_u}{dt} = Vel_u$$

(14)

where β is a damping constant.

Definition of zones in the apical hook model

Predictions of cross-section hook model suggest that auxin transport within the epidermis and cortex tissues is essential to generate auxin maximum on the concave side of the hook (Figure 1A). Because this particular feature of cross-section model is difficult to translate in the 2D longitudinal hook model, we chose to model an approximate scenario; such that auxin might leave the epidermis on the convex side of the hook and re-enter the epidermis on the concave side of the hook and vice versa. Because there are more PINs on the convex side of the hook that auxin will preferentially travel to the concave side of the hook. This simplified solution mimics an auxin flow within the epidermis in our 2D apical hook model.

Cell association to three different zones of the model (Figure 3A) was obtained by

calculating the relative distance of each cell from the cotyledons (uppermost cell layer, Figure 3A). We have chosen to use relative distances since they represent more realistic scenario as the hook apex consist of cell populations which constitutively divides and grows. Therefore the hook zone is dynamically adapted during apical hook formation. This is different from scenario in plant leaves where the absolute distances from the leaf base determines the geometry of the leaf [S15]. These distances were calculated by adding lengths of linear Hookean springs anchored to the beginning of the apex and were afterwards normalized in the (0, 1) range. Next, two cut-off values for these distances were defined; one associated with the beginning of hypocotyl region (D_{hyp}) and the other one associated with the end of cotyledon zone (D_{cot}). To define the zone of rapid cell division the distance threshold D_{div} was used. For values of distance thresholds and other model parameters we refer to Supplemental Table 2.

Definition of cell growth

To model local, longitudinal growth of the tissue, we assumed that the rest length of each linear spring increases over time according to the following heuristic formula:

$$\frac{dL_{u,v}}{dt} = L_{u,v} \cdot \left[r_b + z(\overline{AUXIN_{u,v}}) \right] \quad (15)$$

where r_b is a isotropic growth rate and $z(\overline{AUXIN_{u,v}})$ is the anisotropic growth rate (longitudinal growth) that depends on the mean auxin concentration in two adjacent cells that share the common spring interface. Therefore, the cell growth rate decreases when auxin concentrations increase (Supplemental Figure 10), as observed experimentally [S16]:

$$z(\overline{AUXIN_{u,v}}) = \frac{a}{1 + b \cdot exp^{c \cdot \overline{AUXIN_{u,v}}}} \quad (16)$$

Default cell division occurs once cells reach a certain area threshold. In the zone of rapid cell division we assumed cell area threshold of 900 μm^2, elsewhere it is 2500 μm^2. The auxin-concentration threshold for auxin-induced cell divisions used in simulations in Supplemental Figure 6F-6H was set to 500 [*n*M]. With each cell division event forces that act on daughter cell walls are relaxed and thus rapidly reach the equilibrium. As consequence the proliferating cells on the concave side are initially relaxed whereas the cells on the convex side of the hook undergo rapid outgrowth leading to the further hook bending.

Supporting References

S1. **Smith C, Prusinkiewicz P, and Samavati F.** (2003) Local specification of surface subdivision algorhithms. *Lecture Notes in Computer Science* **3062**: 313–327

S2. **Smith RS, Guyomarc'h S, Mandel T, Reinhardt D, Kuhlemeier C, and Prusinkiewicz P.** (2006) A plausible model of phyllotaxis. *Proc. Natl. Acad. Sci.* **103**: 1301–1306

S3. **Karwowski R, and Prusinkiewicz P.** (2004) The L-system-based plant-modeling environment L-studio 4.0. *In Proceedings of the 4th International Workshop on Functional-Structural Plant Models*, pp. 403-405

S4. **Prusinkiewicz P.** (2004). Art and science for life: Designing and growing virtual plants with L-systems. *ActaHortic*, **630**: 1528

S5. **Press WH, Teukolsky SA, Vetterling WT, Flannery BP** (1992) *Numerical recipes in C (2nd ed.): the art of scientific computing*: Cambridge University Press. 994 p.

S6. **Goldsmith MH, Goldsmith TH, & Martin MH.** (1981) Mathematical analysis of the chemosmotic polar diffusion of auxin through plant tissues. *Proc. Natl. Acad. Sci.* **78**:976-980.

S7. **Grieneisen VA, Xu J, Maree AF, Hogeweg P, & Scheres B.** (2007) Auxin transport is sufficient to generate a maximum and gradient guiding root growth. *Nature* **449**:1008-1013

S8. **Swarup R**, *et al.* (2005) Root gravitropism requires lateral root cap and epidermal cells for transport and response to a mobile auxin signal. *Nat Cell Biol* **7**:1057-1065.

S9. **Kramer, EM, Rutschow, HL &Mabie, SS.** (2011) AuxV: a database of auxin transport velocities. *Trends Plant Sci* **16**: 461-463.

S10. **Žádníková P, Petrášek J, Marhavý P, Raz V, Vandenbussche F, et al.** (2010) Role of PIN-mediated auxin efflux in apical hook development of Arabidopsis thaliana. *Development* **137**: 607-617.

S11. **F. D. Fracchia, P. Prusinkiewicz, and M. J. M. de Boer** (1990) Animation of the development of multicellular structures, *in Computer Animation* '90, N. Magnenat-Thalmann and D. Thalmann, eds., Tokyo, 1990, Springer-Verlag, pp. 3–18.

S12. **Prusinkiewicz, P. and A. Lindenmayer** (1990). The algorithmic beauty of plants**,** *Springer-Verlag New York, Inc.*

S13. **Matthews, MJ.** (2002). Title: „Physically Based Simulation of Growing Surfaces". Master degree thesis. Department of Computer Science, University of Calgary, Alberta.

S14. **Smith, RS.** (2011) Modeling Plant Morphogenesis and Growth. In "New Trends in the Physics and Mechanics of Biological Systems: *Lecture Notes of the Les Houches Summer School*: Volume 92, July 2009, Oxford University Press, 2011.

S15. **Kuchen EE, Fox S, de Reuille PB et al.** (2012) Generation of leaf shape through early patterns of growth and tissue polarity. *Science* **335**: 1092-1096

S16. **Perrot-Rechenmann C** (2010) Cellular responses to auxin: division versus expansion. *Cold Spring Harb Perspect Biol* **2**: a001446.